Cancer Nanotechnology

RESEARCH Open Access

Carboxylated graphene quantum dots-mediated photothermal therapy enhances drug-membrane permeability, ROS production, and the immune system recruitment on 3D glioblastoma models

Giordano Perini[1,2], Valentina Palmieri[2,3], Ginevra Friggeri[1], Alberto Augello[2], Marco De Spirito[1,2] and Massimiliano Papi[1,2*]

*Correspondence:
Massimiliano.papi@unicatt.it

[1] Dipartimento di Neuroscienze, Università Cattolica del Sacro Cuore, Largo Francesco Vito 1, 00168 Rome, Italy
[2] Fondazione Policlinico Universitario A. Gemelli IRCSS, 00168 Rome, Italy
[3] Istituto dei Sistemi Complessi, CNR, Via dei Taurini 19, 00185 Rome, Italy

Abstract

Graphene quantum dots (GQDs) are biocompatible nanoparticles employed in biomedical field, thanks to their size and photophysical properties. GQDs have shown the capability to cross biological barriers, including the blood–brain barrier, which makes them promising agents for brain diseases therapy. It has been shown that surface-functionalized GQDs enhance membrane fluidity and intracellular uptake, exerting a synergistic effect with antitumor drugs at subtherapeutic doses. Here, we tested GQDs effects in combination with chemotherapeutic agents doxorubicin and temozolomide, on a complex 3D spheroid model of glioblastoma. We observed that the capability of GQDs to absorb and convert near-infrared light into heat is a key factor in membrane permeability enhancement on 3D model. This non-invasive therapeutic strategy named photothermal therapy (PTT), combined to chemotherapy at subtherapeutic doses, significantly increased the effect of antitumor drugs by reducing tumor growth and viability. Furthermore, the increase in membrane permeability due to GQDs-mediated PTT enhanced the release of reactive oxygen species with strong migration of the immune system towards irradiated cancer spheroids. Our data indicate that the increase in membrane permeability can enhance the efficacy of antitumor drugs at subtherapeutic doses against glioblastoma, reducing side effects, and directing immune response, ultimately improving quality of life for patients.

Keywords: Graphene, Glioblastoma, Photothermal, Photodynamic, 3D-bioprinting

Background

Graphene quantum dots (GQDs) are small semiconducting nanoparticles with a size around 10 nm (Perini et al. 2020b). Thanks to their great photophysical properties, GQDs have widely been exploited in several fields (Perini et al. 2020b; Huang et al. 2014). GQDs have been employed as bioimaging molecules, carriers for drug

delivery, and as theranostic nanomolecules (Bacon et al. 2014; Mansur 2010). Thanks to their capability of easily crossing biological barriers, particularly the blood–brain barrier, GQDs are also being used in the field of neuroscience (Hanada et al. 2014; Utkin 2018). In our previous works, we have tested the effect of surface-chemically functionalized biocompatible GQDs in combination with chemotherapy on a traditional 2D model of glioblastoma, the most lethal and aggressive brain cancer (Perini et al. 2020a, c). We demonstrated that GQDs functionalized with carboxylic acid could synergistically enhance chemotherapy against glioblastoma (Perini et al. 2020c). However, an issue that still must be overcome is the lack of reliable experimental models, different from standard 2D cultures, to provide representation of tumor' behavior (Perini 2021a). We observed that this synergistic tumor killing efficacy of GQDs and chemotherapy was reduced on 3D glioblastoma spheroids indeed (Perini et al. 2022a). We therefore exploited another photophysical property of GQDs: the capability of absorbing near-infrared light and convert it into heat, namely phototherapy. Phototherapy, which comprises photothermal therapy (PTT) and photodynamic therapy (PDT), is a non-invasive treatment that can either sensitize cells to chemotherapy by inducing a local increase of temperature mediated by light and that can induce a local increase in the production of reactive oxygen species, respectively (Perini et al. 2022b; Liu et al. 2020a; Zhi et al. 2020). Here, we tested GQDs-mediated combined chemotherapy and phototherapy on a reliable 3D tumor spheroid model of glioblastoma. For this purpose, we focused on GQDs functionalized with carboxylic acid groups (Perini 2021b). We demonstrated that GQDs exert a strong killing effect as a chemo-photosensitizer agent on tumor spheroids when combining chemotherapy with an approach based on hyperthermia. We observed that the increase in efficacy of tumor killing was related to a strong increase in membrane permeability induced by GQDs and, in particular, by irradiated GQDs. We therefore proposed a mechanism of action in which the increase in membrane permeability induced by GQDs improves intracellular uptake of antitumor drugs inside glioblastoma cells (Perini et al. 2020a, c; Sui, et al. 2016). Another relevant approach for the treatment of glioblastoma is immunotherapy (Ampie et al. 2015; Lim et al. 2018; Qian and Shao 2022) due to the paucity of infiltrated leukocytes and downregulation of immunological response, facilitated by intratumoral heterogeneity (Ampie et al. 2015). The purpose of immunotherapy is to reactivate the immune system, stimulating it to recognize tumor-associated antigens, in order to directly target tumor region, minimizing the non-specific inflammatory response. For this purpose, PTT and PDT can be auxiliary approaches for immunotherapy, due to the high release of tumor-associated antigens and the production of reactive oxygen species, which induce a strong activation of the immune system (Kim and Lee 2018; Rubenstein et al. 2000). Here, we observed a strong migration of immune cells towards cancer region after irradiation with a near-infrared laser in the presence of GQDs. Taken together, our findings on a reliable 3D tumor model demonstrate the crucial clinical relevance of GQDs, which could take part in the fight against brain diseases thanks to their multifunctional chemo-photosensitizing effect, and to their ability of stimulating the migration of immune cells towards cancer region, exerting immunotherapy enhancement.

Results

Characterization of GQDs

GQDs were characterized by DLS, TEM, AFM, absorbance, fluorescence intensity, and ATR-FTIR. Results of spectroscopic and microscopic characterization are reported in Fig. 1. TEM images depicted an average diameter of GQDs around 10 nm (Fig. 1A), which is in accordance with DLS analysis that showed a broad size distribution having a hydrodynamic radius peaked at 6 nm (Fig. 1B). Absorbance measurements were performed by recording optical density (OD) from 230 to 800 nm (Fig. 1C). We observed a peak at 350 nm, which is typically due to $\pi-\pi*$ transitions, and it is associated with the presence of lone pairs within oxygens. Fluorescence intensity was recorded by exciting from 260 to 480 nm with a step size of 20 nm and reading emission from 300 to 700 nm with a step size of 5 nm (Fig. 1D). AFM imaging along with analysis of line profile was performed on samples. Results are reported in Fig. 1E, F, furtherly confirming TEM results. GQDs showed an emission peak at 450 nm when excited at 320 nm. Surface chemical characterization was performed by ATR-FTIR (Fig. 1G). The infrared spectra of GQDs showed characteristic frequencies of the carboxylic acid group, such as a broad band around 3000 cm^{-1} for the O–H stretch and a very strong band at 1705 cm^{-1} for the C=O stretch. Furthermore, we observed a peak at 1200 cm^{-1} due to epoxide C–O stretching vibrations. We then evaluated the biocompatibility of GQDs on the U87 human glioblastoma cell line and on human fibroblasts to confirm the high

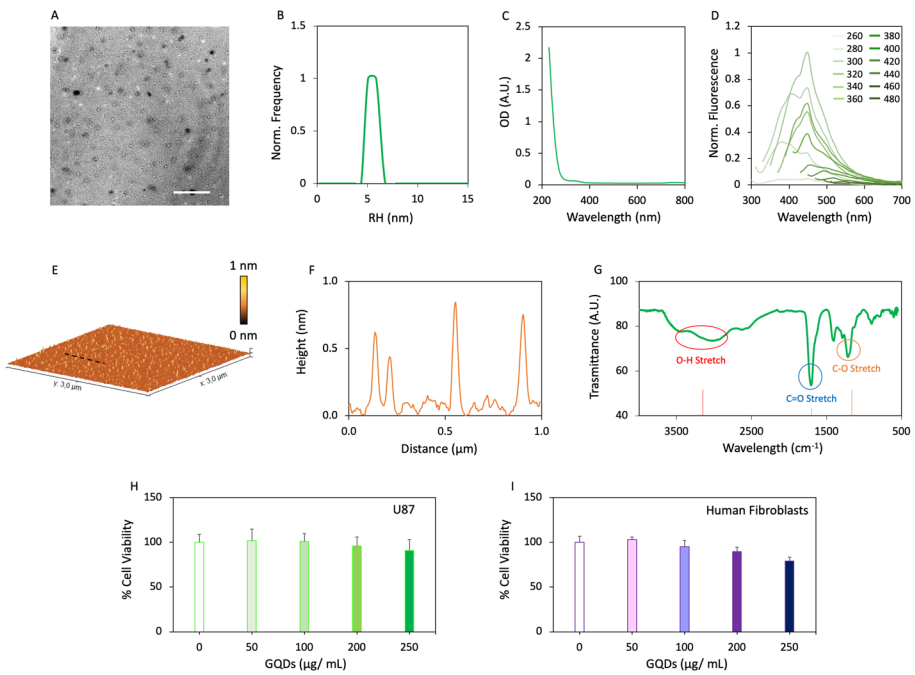

Fig. 1 Characterization of GQDs. **A** TEM imaging of GQDs, showing a diameter around 10 nm. Scalebar 50 nm. **B** Light scattering measurements of GQDs, depicting a hydrodynamic radius around 6 nm. **C** Absorbance of GQDs in the range between 230 and 800 nm. **D** Fluorescence intensity of GQDs by exciting from 260 to 480 nm and recording emission from 300 to 700 nm. **E** AFM images of GQDs and **F** representative line profile of the image. **G** FTIR spectroscopy showing typical peaks of GQDs functionalized with carboxyl groups. **H**, **I** Biocompatibility of GQDs on glioblastoma cells and human fibroblasts, respectively, at concentrations ranging from 50 to 250 μg/mL. Results are reported as % of control (untreated) cells

biocompatibility of these nanomaterials. We administered GQDs at different concentrations, ranging from 50 to 250 μg/mL. Results are reported in Fig. 1H, I. No evident cytotoxicity was depicted even at the highest tested concentration, highlighting the biocompatibility of bare GQDs.

Effect of changes in membrane permeability mediated by GQDs on 2D model of glioblastoma

We then moved to evaluate the effect of GQDs on changes in the permeability of cell membrane, to test whether these changes could improve the effect of two chemotherapeutic agents: temozolomide (TMZ) and doxorubicin (DOX). For this purpose, we administered GQDs to cells and, after incubation, we labeled cells with Laurdan (Parasassi et al. 1990, 1998). This molecule is a fluorescent probe with a hydrophilic head and a hydrophobic tail that can be used to describe the lipid-phase state in membranes with high sensitivity. Membrane fluidity quantified by Laurdan is given by calculation of the generalized polarization (GP) index, which goes from −1 (highest membrane fluidity) to +1 (lowest membrane fluidity) (Bianchetti et al. 2019). Representative Laurdan confocal microscopy images are reported in Fig. 2A, while quantification of the GP is shown in Fig. 2B. Data are reported as mean ± standard deviation. We observed a GP value of 0.48 ± 0.05 for control (untreated) U87 cells. Cells treated with GQDs had a GP value of 0.21 ± 0.02. Cells treated with GQDs showed a GP value significantly lower than control cells, highlighting a strong increase in membrane fluidity ($p < 0.01$, one-way ANOVA and Tukey post-hoc test). We then moved to test the combined effect of GQDs and the two chemotherapeutics, to test whether the increase in membrane permeability could augment the effectiveness of the antitumor drugs due to a higher intracellular uptake. First, we evaluated the concentration of chemotherapeutic agent capable of inhibiting 50% of cell growth (namely IC50). Data for DOX are reported in Fig. 2C. We observed a reduction in cell viability corresponding to the IC50 at 2 μM. We then set the concentration of DOX in combination with GQDs at a subtherapeutic dose, which was half of the IC50 (1 μM). We incubated cells with GQDs at concentration ranging from 50 up to 250 μg/mL for 24 h. After incubation, we removed GQDs from the supernatant to avoid possible extracellular interactions between GQDs and antitumor drugs that could affect the effectiveness of the latter. We then added DOX at half of its IC50. After further incubation, we measured cell viability. Results of the combined effect of GQDs and DOX are reported in Fig. 2D as % of death (1-viability). DOX and GQDs at 50 μg/mL depicted a cell mortality of 37 ± 7.1%. This reduction was similar to that of DOX alone. We observed a strong reduction in viability with the combined treatment of GQDs at concentrations higher than 50 μg/mL and DOX compared to the anticancer drug alone. Mortality resulted significantly higher for cells treated with DOX and GQDs at the two highest tested concentrations (200 and 250 μg/mL, with a $p < 0.01$, one-way ANOVA and Tukey post-hoc test). To verify the hypothesis of a higher intracellular uptake of the antitumor drug, we evaluated the fluorescence intensity of DOX inside cells through confocal microscopy. Results of the fluorescence intensity are reported in Fig. 2E. We observed a significant increase in the fluorescence intensity of DOX inside cells at the two highest tested concentrations, in accordance with cell viability. Our data show a

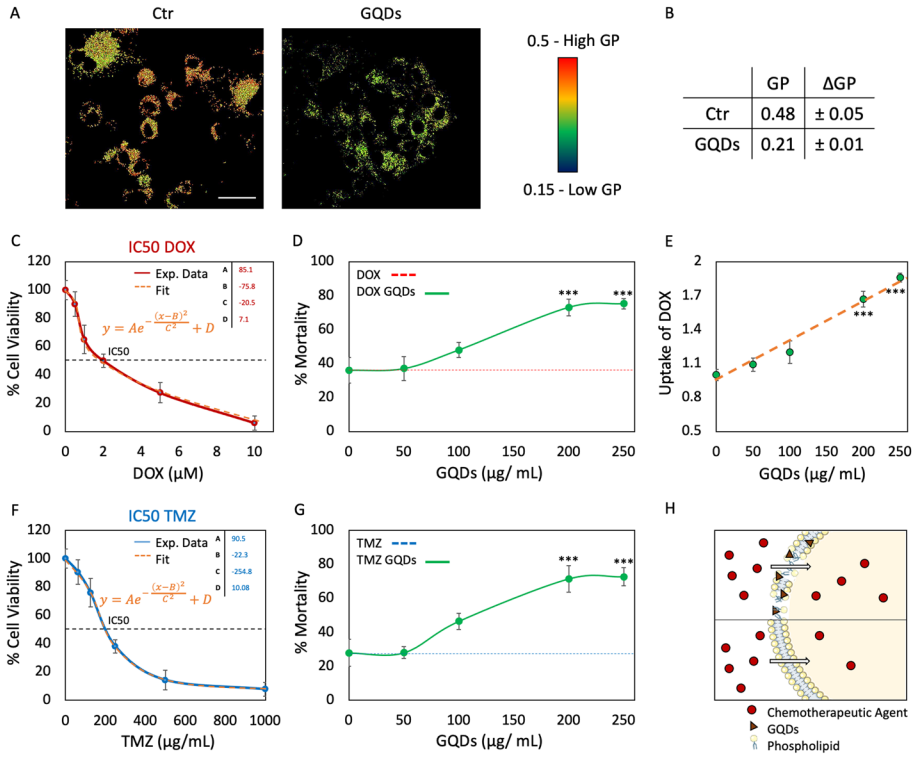

Fig. 2 Mechanism of GQDs-mediated chemotherapy enhancement. **A** Laurdan confocal microscopy images of cells treated with GQDs. Scale bar 20 μm. **B** Quantification of the generalized polarization (GP) of glioblastoma cells after the treatment with GQDs. **C** Dose–response curve of doxorubicin (DOX), highlighting a concentration inhibiting 50% of cell growth (IC50) at 1 μM. **D** Mortality of glioblastoma cells after the combined treatment with GQDs and DOX at half of its IC50. **E** Quantification of the uptake of DOX inside glioblastoma cells. **F** Dose–response curve of doxorubicin (DOX), highlighting a concentration inhibiting 50% of cell growth (IC50) at 200 μg/mL. **G** Mortality of glioblastoma cells after the combined treatment with GQDs and TMZ at half of its IC50. **H** Proposed mechanism of action on the combined treatment between GQDs and anticancer drugs. GQDs tend to destabilize cell membrane, increasing membrane permeability. This allows a higher uptake of antitumor molecules, improving their efficacy. ***$p < 0.01$ one-way ANOVA and Tukey post-hoc test

clear correlation between intracellular uptake of the anticancer drug and changes in membrane permeability due to the treatment of GQDs. Therefore, we moved to test the effectiveness of TMZ, since it is known to be the most widely used chemotherapy for patients with glioblastoma (Stupp et al. 2005; Jiapaer et al. 2018; Lee 2016). As for DOX, we first evaluated the IC50 of TMZ, which resulted to be 200 μM (Fig. 2F). We then proceeded with the same experimental protocol of DOX. We administered GQDs at the same previous concentrations, then after incubation we removed GQDs from supernatant and we dispensed TMZ at half of its IC50. Results are reported in Fig. 2G. As for DOX, no significant changes in mortality were pointed out after administration of GQDs at the lowest concentration of μg/mL when compared to TMZ alone. As expected, the combined treatment of GQDs and TMZ resulted in a significant effect at the two highest tested concentrations of GQDs ($p < 0.01$, one-way ANOVA and Tukey post-hoc test). Our data strongly indicate that biocompatible GQDs can interact with cell membrane in a concentration-dependent manner. This interaction leads to an increase in membrane permeability, due to a higher membrane

fluidity that we measured through GP. The changes in membrane permeability allow the entrance of the chemotherapeutic agent, significantly enhancing its efficacy (Fig. 2H).

Effect of the combined treatment of GQDs and chemotherapy on a 3D model of glioblastoma

We have tested the effect of GQDs in combination with chemotherapy on a 2D model of glioblastoma. We demonstrated that GQDs could synergistically enhance chemotherapy against cancer. We explained the mechanism underlying the synergy between GQDs and antitumor drugs by measuring an increased membrane permeability of U87 cells. However, an issue that still must be overcome is the lack of reliable experimental models, different from standard two-dimensional cultures, to provide a faithful representation of tumor behavior (Pierangeli et al. 2020; Longati et al. 2013; Costa et al. 2016). For this purpose, we moved to test the enhancement of chemotherapy mediated by changes in membrane permeability induced by GQDs on a reliable 3D tumor spheroid model of glioblastoma. We monitored spheroid growth in terms of size and viability for a timespan of two weeks. Results are reported in Fig. 3. Spheroid growth was monitored in the timespan of two weeks for all treatments by acquiring bright field images over time (Fig. 3A). After the formation of spheroids, we administered GQDs at 200 µg/mL. After incubation, we administered antitumor drugs. Results of the combined treatment of GQDs and DOX in terms of spheroid growth are reported in Fig. 3B. Data are normalized by the area at day 0 for each treatment. Control (untreated) spheroids increased their size up to 173 ± 10.4%. Spheroids treated with GQDs showed a similar increase in their size, reaching 152 ± 11.1%. The chemotherapeutic drug alone exerted a reduction in spheroid growth over time, decreasing to 78 ± 7.6% with respect to the initial size. Importantly, the most evident effect was exerted by the coadministration of GQDs and DOX. Spheroids treated with the combination of DOX and GQDs had a reduction in their growth to 73 ± 2.8% indeed. Both treatments with DOX and GQDs combined

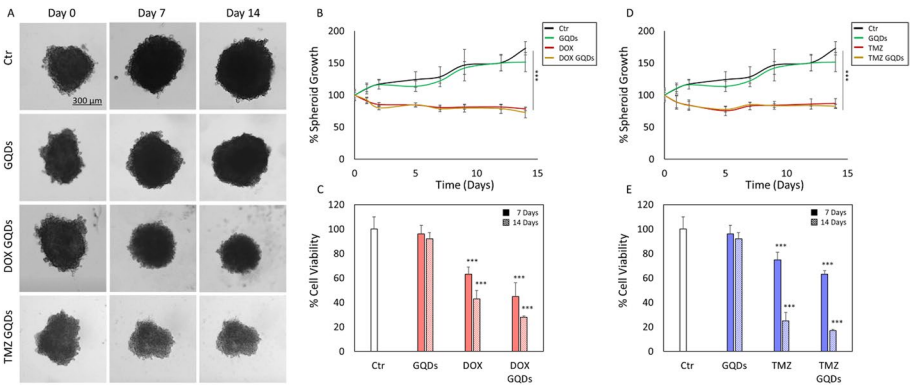

Fig. 3 Combined effect of GQDs and chemotherapy on spheroid models of glioblastoma. **A** Bright field images of spheroids at 0, 7, and 14 days from administration of GQDs. **B** Growth of spheroids treated with GQDs and DOX. **C** Cell viability of spheroids treated with GQDs and DOX at 7 and 14 days from administration of GQDs. **D** Growth of spheroids treated with GQDs and temozolomide (TMZ). **E** Cell viability of spheroids treated with GQDs and TMZ at 7 and 14 days from administration of GQDs. ***$p < 0.01$ one-way ANOVA and Tukey post-hoc test

with DOX resulted in a significant loss of tumor mass when compared to untreated spheroids ($p < 0.01$, one-way ANOVA and Tukey post-hoc test). However, despite experimental evidence on 2D model, no significant difference between the two groups was observed on spheroids. Results of cell viability at 7 and 14 days from administration of GQDs are reported in Fig. 3C as % of control spheroids. Spheroids treated with GQDs at 7 and 14 days did not show relevant loss in viability. Spheroids treated with DOX alone at half of its IC50 had a reduction in cell viability up to $63 \pm 10.3\%$ and $43 \pm 2.1\%$ at 7 and 14 days, respectively. Spheroids treated with the combination of GQDs and DOX depicted a loss of viability at 7 and 14 days up to $45 \pm 7.6\%$ and $28 \pm 3.1\%$, respectively. Both treatments with DOX alone or in combination with GQDs resulted in a significant loss in cell viability with respect to control (untreated) spheroids ($p < 0.01$, one-way ANOVA and Tukey post-hoc test). Although there was a clear decreasing trend, in accordance with the data of tumor growth, indicating an enhanced efficacy of the antitumor drug in the presence of GQDs, we did not observe significant differences between the two treatment groups. As for the 2D model, we then moved to test the combined effect of GQDs and TMZ. Results of spheroid growth are reported in Fig. 3D. After two weeks, glioblastoma spheroids treated with TMZ had a reduction in their growth up to $87 \pm 8.3\%$. When TMZ was combined with GQDs, spheroids reduced their growth to $83 \pm 2.8\%$. Both treatments resulted to be significantly different with respect to control spheroids ($p < 0.01$, one-way ANOVA and Tukey post-hoc test). Even in this case, we did not observe significant differences between the two treatment groups. Results of cell viability after the treatment with TMZ and GQDs at 7 and 14 days are reported in Fig. 3E. Spheroids treated with the antitumor drug alone had a loss in viability to $75 \pm 3.3\%$ and $25 \pm 1.2\%$ at 7 and 14 days, respectively. Spheroids treated with TMZ and GQDs showed a reduction in viability to $63 \pm 6.1\%$ and $17 \pm 0.4\%$ at 7 and 14 days, respectively. Both treatments significantly reduced cell viability of spheroids ($p < 0.01$, one-way ANOVA and Tukey post-hoc test). As for DOX, despite the decreasing trend indicating an enhanced efficacy of TMZ in combination with GQDs, we did not observe significant differences between the two treatment groups.

Increase in membrane permeability of glioblastoma spheroids through photothermal conversion mediated by GQDs

We have tested coadministration of GQDs and antitumor drugs on a tumor spheroid, which allows reproducing a more reliable model of glioblastoma with respect to standard cultures. As a fact, several studies reported that most of the tests carried out on 2D models show a significant change in their outcomes when compared to 3D cultures (Perini et al. 2022a; Longati et al. 2013; Costa et al. 2016; Moriconi 2017; Pickl and Ries 2009; Jauković et al. 2020; Sánchez-Romero et al. 2016). Therefore, a multidisciplinary approach for the treatment of glioblastoma, which guarantees effective tumor cell targeting and killing and is coupled with an efficient experimental model is mandatory. For this purpose, we exploited another feature of GQDs, which is their ability to absorb near-infrared (NIR) light and convert it into heat, exerting a photothermal effect (Perini et al. 2022a; Wang et al. 2019; Sung et al. 2017; Liu et al. 2020b). This effect can be used in a therapeutic approach, namely PTT. PTT is a non-invasive technique that can be an intriguing auxiliary approach for chemotherapy. PTT is based on a local increase in

temperature mediated by light-responsive molecules, which in turn exerts a cytotoxic effect on cancer cells. GQDs have widely demonstrated their high photothermal conversion (Wang et al. 2019; Nurunnabi et al. 2014). Therefore, in this work, we used GQDs as chemotherapy enhancers and photothermal converting molecules (Fig. 4A). For this purpose, we used a near-infrared laser, with an emission wavelength of 808 nm. Characterization of the laser power is reported in Fig. 4B. Once characterized, we irradiated GQDs at all tested concentrations for 5 min at a power density of 6 W/cm^2, in accordance with previous data (Perini et al. 2022a; Rosenkranz et al. 2021). We found a concentration-dependent increase in temperature over time. GQDs at 50 µg/mL increased local temperature from RT (25 °C) up to 28 °C after 5 min of irradiation, similar to the culture medium alone. GQDs at 100 µg/mL depicted a higher temperature raise up to 38 °C. GQDs at the two highest tested concentrations (200 and 250 µg/mL) showed a similar increase in temperature up to 46 and 49 °C, respectively. Therefore, we performed further experiments by setting our working concentration of GQDs at 200 µg/mL. It has already been hypothesized that a mild near-infrared irradiation can induce an augmented membrane permeability. Therefore, we tested the capability of GQDs to increase

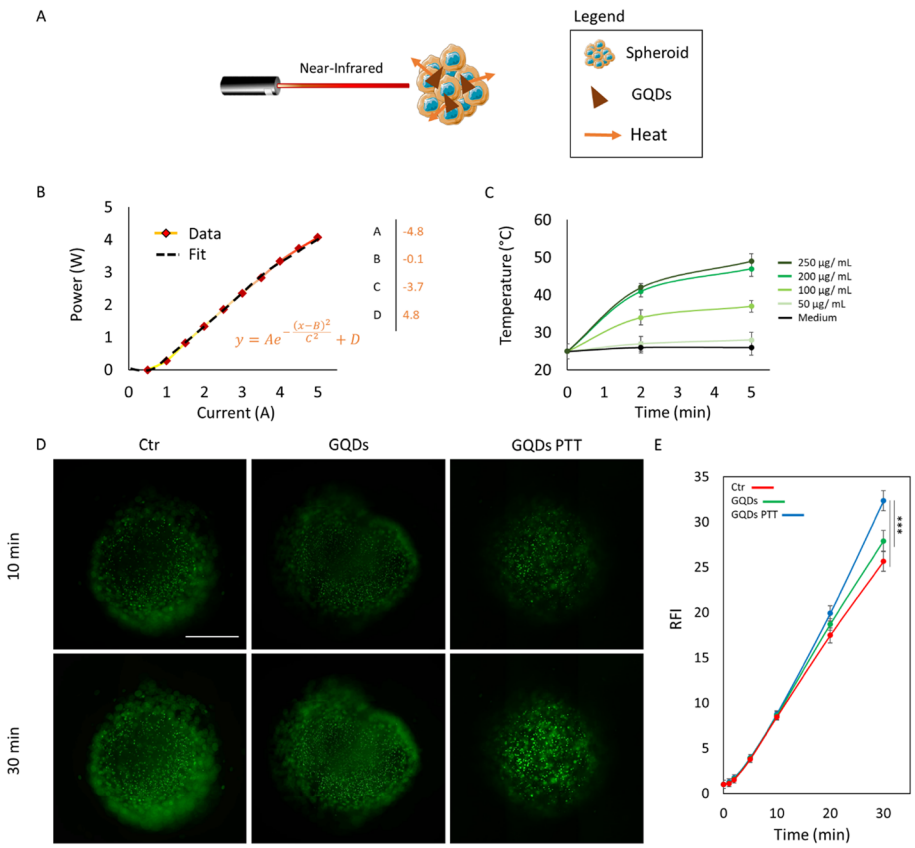

Fig. 4 Photothermal enhancement of membrane permeability on glioblastoma spheroids through GQDs. **A** Schematic representation of photothermal therapy (PTT) exploiting GQD as photosensitizing agents. **B** Characterization of the 808 nm laser used for PTT. **C** Thermal conversion of GQDs at different concentrations. **D** Fluorescence imaging of calcein entering through glioblastoma spheroids. Scale bar 200 µm. **E** Fluorescence intensity of calcein inside glioblastoma spheroids after photothermal treatment through GQDs, measured in a time span of 30 min, indicating a significant increase in membrane permeability. ***$p < 0.01$ one-way ANOVA and Tukey post-hoc test

the membrane permeability after photothermal conversion. For this purpose, we administered GQDs to glioblastoma spheroids and, after incubation, we irradiated them with the 808 nm laser. We then administered calcein to spheroids in order to monitor its uptake (Fig. 4D). Results of calcein uptake are reported in Fig. 4E. Results are reported as fluorescence intensity of each group normalized by its intensity at the beginning of the experiment. After 30 min, fluorescence intensity of calcein in spheroids treated with GQDs and irradiated with near-infrared laser was 32 ± 1.6 times higher compared to t0. Fluorescence intensity of spheroids treated with only GQDs had an increase of 27 ± 1.3 with respect to t0. We observed a significant increase in fluorescence intensity of calcein in spheroids treated with GQDs and irradiated ($p < 0.01$, one-way ANOVA and Tukey post-hoc test). Taken together, our data suggest that GQDs can increase membrane permeability even in a reliable 3D tumor spheroid model through photothermal conversion.

Photothermal-enhanced chemotherapy through GQDs on glioblastoma spheroids

We therefore repeated our experiment of chemotherapy enhancement on glioblastoma spheroids by implementing PTT. We administered GQDs and, after incubation, we added the antitumor drugs. We then irradiated spheroids with near-infrared light, and we evaluated the combined effect of PTT and chemotherapy in terms of spheroid growth and reduction of cell viability. Data are reported in Fig. 5 for both DOX and TMZ. We acquired bright field images of spheroids over time for all treatments (Fig. 5A), from which we evaluated spheroid growth in the same time span of 2 weeks. Results of spheroid growth after the treatment with GQDs-mediated PTT and DOX are reported in Fig. 5B. Administration of GQDs and consequent PTT slackened spheroid growth to $115 \pm 11.1\%$ with respect to their initial size. Spheroids treated with photothermal-mediated enhancement of chemotherapy through GQDs had a critical reduction in spheroid growth to $40 \pm 5.7\%$. Both GQDs-mediated PTT and photothermal-mediated enhancement of chemotherapy were significantly different from control untreated spheroids ($p < 0.01$, one-way ANOVA and Tukey post-hoc test). Importantly, the combination of

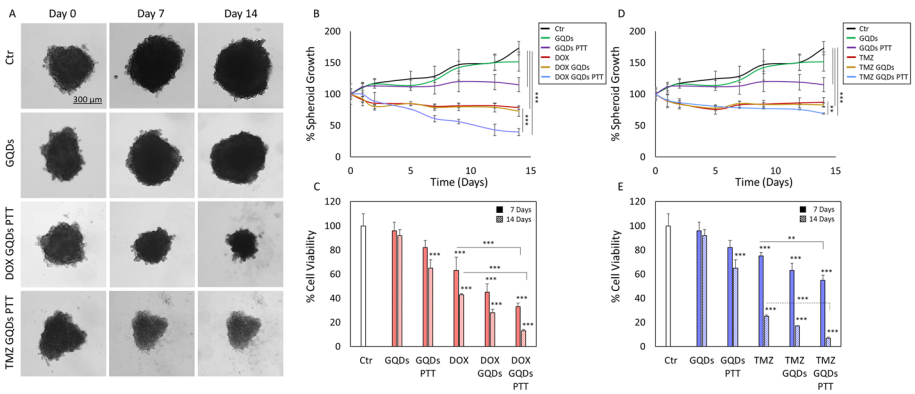

Fig. 5 Combined effect of GQDs-mediated PTT and chemotherapy on spheroid models of glioblastoma. **A** Bright field images of spheroids at 0, 7, and 14 days from administration of GQDs. **B** Growth of spheroids treated with GQDs-mediated PTT and DOX. **C** Cell viability of spheroids treated with GQDs-mediated PTT and DOX at 7 and 14 days from administration of GQDs. **D** Growth of spheroids treated with GQDs-mediated PTT and TMZ. **E** Cell viability of spheroids treated with GQDs-mediated PTT and TMZ at 7 and 14 days from administration of GQDs. $^{**}p < 0.05$ and $^{***}p < 0.01$ one-way ANOVA and Tukey post-hoc test

PTT and chemotherapy was significantly more effective than the antitumor drug alone or coadministrated with GQDs. Viability measurements furtherly confirmed the effectiveness of PTT and chemotherapy (Fig. 5C). We observed a reduction in viability of cells treated with GQDs and irradiated. This was particularly evident at 14 days from administration, which resulted in a loss of viability to $65 \pm 7.1\%$ with respect to control spheroids ($p < 0.01$, one-way ANOVA and Tukey post-hoc test). PTT through GQDs combined with DOX exerted a strong reduction at both 7 and 14 days from administration of GQDs, resulting in $33 \pm 3.1\%$ and $13 \pm 3.2\%$, respectively. Importantly, this combined treatment was significantly more effective than the chemotherapeutic drug alone ($p < 0.01$, one-way ANOVA and Tukey post-hoc test). We then moved to test TMZ combined with GQDs-mediated PTT. Results of spheroid growth are reported in Fig. 5D. Spheroids treated with the combination of TMZ and PTT had a significant reduction in spheroid growth to $69 \pm 1.1\%$ compared to the initial size and to the antitumor drug alone. Cell viability furtherly confirmed the data of TMZ and PTT (Fig. 5E), highlighting a reduction of up to $55 \pm 4.6\%$ and $7 \pm 0.4\%$ at 7 and 14 days, respectively. As for DOX, this loss in viability was significant at both 7 and 14 days with respect not only to control spheroids, but also to TMZ alone ($p < 0.05$ and $p < 0.01$, one-way ANOVA and Tukey post-hoc test). Taken together, our data indicate that GQDs alone are not capable of significantly changing membrane permeability on a reliable model. However, by exploiting the photothermal conversion ability of these nanoparticles, it is possible to alter the membrane permeability on a reliable spheroid model by increasing the efficacy of antitumor drugs.

Increase in spheroid membrane permeability through GQDs-mediated PTT induce an improved uptake of chemotherapy

We hypothesized that the lack of effectiveness in absence of PTT could be due to a poor penetration capability of chemotherapeutic agents through the core of spheroids (Perini 2021a; Priwitaningrum et al. 2016; Bugno et al. 2016; Lazzari et al. 2019; Ma et al. 2012). Therefore, we measured the penetration depth of DOX along with its uptake inside spheroids after PTT. For this purpose, we administered GQDs and, after incubation, we added DOX. We then irradiated spheroids, and we measured the penetration of DOX and its fluorescence intensity. Results are reported in Fig. 6. Figure 6A depicts representative confocal microscopy images of spheroids incubated with DOX. When treated with PTT-enhanced chemotherapy, spheroids displayed a significantly higher penetration depth of the antitumor drug with respect to DOX alone or without PTT (Fig. 6B, $p < 0.01$, one-way ANOVA and Tukey post-hoc test). In accordance with penetration depth, fluorescence intensity of DOX was significantly higher in spheroids treated with PTT and DOX (Fig. 6C). These data strongly confirm our proposed mechanism of action of irradiated GQDs, which can induce an increase in membrane permeability of spheroids, improving penetration depth of the antitumor drug, along with its uptake. Taken together, our findings suggest that biocompatible GQDs can increase membrane permeability through photothermal conversion in a reliable tumor model. The change in membrane permeability allows the use of subtherapeutic doses of antitumor drugs, enhancing its efficacy specifically in cancer region and, at the same time, strongly reducing side effects, potentially improving quality of life for patients.

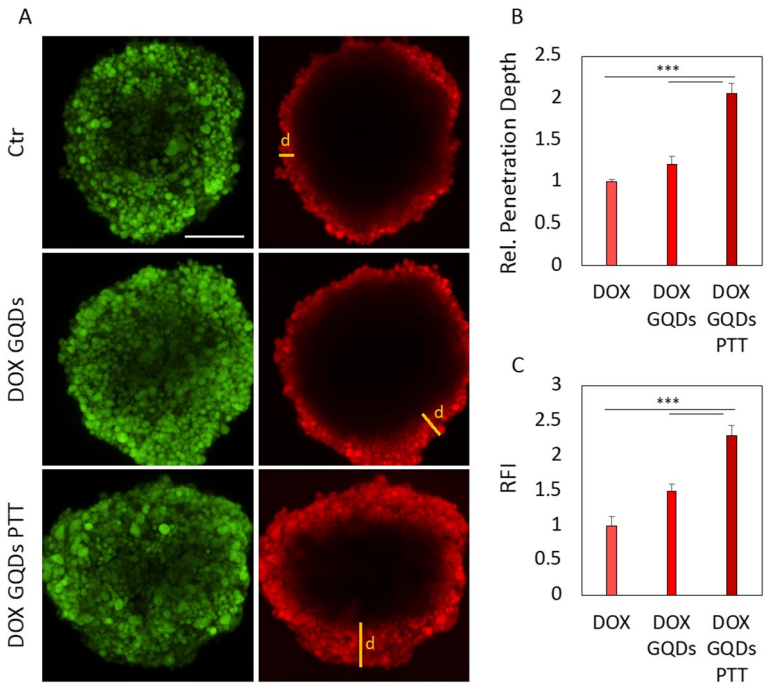

Fig. 6 Penetration of DOX after GQDs-mediated PTT. **A** Representative confocal microscopy images showing spheroid cells labeled with calcein (left) and treated with DOX (red). Scale bar 200 µm. *d* = penetration depth. **B** Penetration depth of DOX within spheroids. Data are normalized by penetration depth of DOX. **C** Fluorescence intensity of DOX inside spheroids. Data are normalized fluorescence intensity of DOX alone. ***$p < 0.01$ one-way ANOVA and Tukey post-hoc test

PTT-mediated induction of migration of immune cells towards cancer region

Another relevant feature of glioblastoma multiforme is the downregulation of immune response (Rubenstein et al. 2000; Forlani et al. 2021; Chongsathidkiet et al. 2018). Glioblastoma-mediated immune suppression is hypothesized to be related to a combination of multiple factors, such as the presence of suppressive CD163+ tumor-associated macrophages or direct induction of apoptosis of leukocytes (Urbańska et al. 2014). Moreover, the high intratumoral heterogeneity of glioblastoma, along with its low number of somatic mutations, furtherly facilitates immune evasion. Immunotherapy aims at reactivating the immune system, stimulating it to recognize tumor-associated antigens, in order to directly target glioblastoma region, minimizing the non-specific inflammatory response that could seriously affect brain architecture and physiology. Recent immune-based therapies have been validated by FDA (Abadi et al. 2021; Heimberger and Sampson 2010; Fecci and Sampson 2019; Woroniecka and Fecci 2018; Anthony et al. 2019; Bausart et al. 2022). Nevertheless, the first clinical trials of immunotherapeutic drugs displayed negative results, mainly due to defects in antigen presentation of tumor associated lymphocytes (Lim et al. 2018). Therefore, auxiliary approaches play a key role to produce specific and long-lasting antitumor immune response against glioblastoma-immune evasion (Bausart et al. 2022). For this purpose, PTT can be an intriguing auxiliary cytotoxic approach for immunotherapy for two main reasons. First, it is known to cause a release of tumor-associated antigens by directly targeting cancer cells (Rong et al. 2019; Chang et al. 2021). Second, depending on the presence of oxygen groups on

the photosensitizing agent, it can induce the production of ROS (Ding et al. 2021; Yang et al. 2019; Sang et al. 2020; Wang et al. 2022; Markovic et al. 2012; Palmieri et al. 2021). Furthermore, increase in membrane permeability due to GQDs-mediated PTT can augment the release of both tumor-associated antigens and ROS produced within cells (Huai et al. 2013; Lemasters 2007; Kowaltowski et al. 2001). For these reasons, we tested the capability of GQDs-mediated PTT to induce migration of immune cells towards cancer region. We performed PTT on glioblastoma spheroids incubated with GQDs and, after the treatment, we co-cultured spheroids with THP-1 human monocytic cells stained in red. We then evaluated migration of immune cells by monitoring red fluorescence intensity in cancer region (Fig. 7A). Results are reported in Fig. 7B, in which the fluorescence intensity is normalized by t0 for each treatment. Importantly, we observed that spheroid's exposure to combination of GQDs-mediated PTT allowed a clearly faster recruitment of immune cells than untreated ones. As described above, the release of tumor-associated antigens and enhanced ROS production are the two main explored mechanisms underlying reactivation of the immune system. Here, we employed GQDs-bearing carboxyl surface functional groups, which are responsible for the production of oxygen species after photothermal treatment (Yao et al. 2020; Palmieri et al. 2019). We evaluated the production of ROS after exposure of spheroids to GQDs-mediated PTT. Results are displayed in Fig. 7C as % of control spheroids. Cells treated with PTT had a clear increase in the production of ROS ($151 \pm 14.7\%$), which was significantly higher than control (untreated) spheroids and than spheroids exposed only to GQDs ($p < 0.01$, one-way ANOVA and Tukey post-hoc test). From this evidence, we can assume that the effect of rapid migration of immune cells is due to a greater production of ROS species.

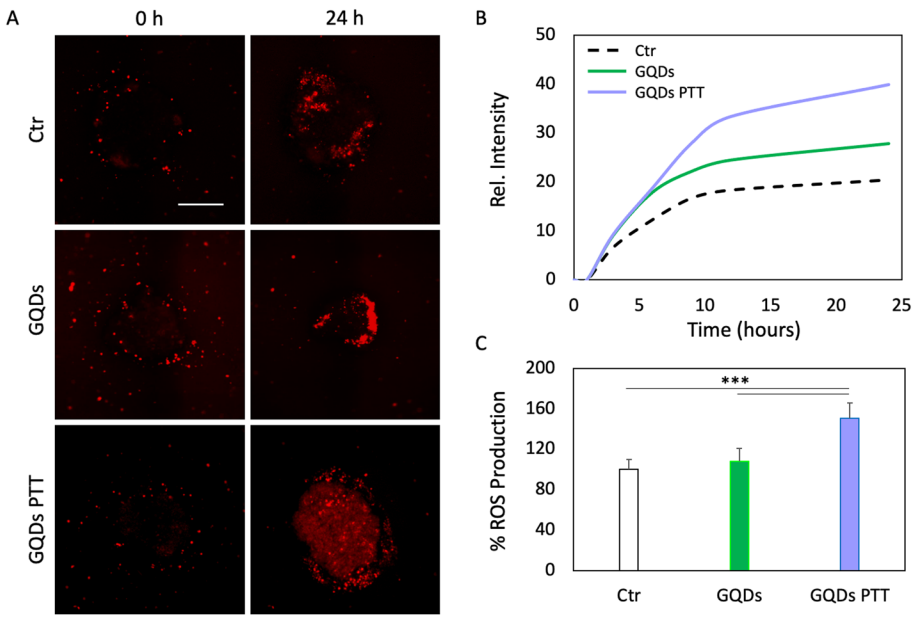

Fig. 7 Migration of immune system towards cancer region mediated by PTT. **A** Representative images of immune cells migrating towards glioblastoma spheroids. Scale bar 200 µm. **B** Fluorescence intensity over time of immune cells in the spheroid area. **C** Production of ROS on glioblastoma spheroids after PTT. ***$p < 0.01$ one-way ANOVA and Tukey post-hoc test

Conclusions

In this work, we tested the effect of GQDs with surface carboxyl groups on glioblastoma multiforme. We demonstrated that GQDs can induce an increase in membrane permeability on a 2D model of brain cancer. We observed that the alteration of membrane permeability enhances the effect of two chemotherapeutic drugs, despite administered at subtherapeutic doses: doxorubicin and temozolomide. We therefore proposed a mechanism of action in which the increase in membrane permeability induced by GQDs improves intracellular uptake of antitumor drugs inside glioblastoma cells. We observed an increased uptake of doxorubicin after exposure of tumor cells to GQDs indeed. We then moved to test the efficacy of GQDs on a more complex and reliable glioblastoma model: 3D cancer spheroids. We monitored the evolution of spheroids exposed to GQDs and the antitumor drugs for two weeks. We observed a strong reduction both in growth and viability. However, this reduction resulted similarly to that of chemotherapeutic drug alone. We hypothesized that GQDs are not capable of inducing a significant change in membrane permeability on a more complex spheroid model. We therefore exploited another feature of GQDs: their capability of absorbing near-infrared light and converting it into heat. This therapeutic approach is called photothermal therapy. We observed that spheroids exposed to GQDs and irradiated with a 6 W/cm^2 near-infrared laser display a significantly higher membrane permeability compared to the treatment with GQDs alone. We then combined GQDs-mediated PTT and chemotherapy at subtherapeutic doses on glioblastoma spheroids. We observed a significant reduction both in spheroid growth and viability in the timespan of two weeks, along with a considerably higher penetration depth and uptake of antitumor drug inside the more reliable glioblastoma model. Taken together, our findings suggest that biocompatible GQDs can increase membrane permeability through photothermal conversion in a reliable tumor model. The change in membrane permeability allows the use of subtherapeutic doses of antitumor drugs, enhancing its efficacy specifically in cancer region and, at the same time, strongly reducing side effects, potentially improving quality of life for patients.

Another crucial issue of glioblastoma is the downregulation of immune response. For this reason, reactivation of the immune response through immunotherapy represents an intriguing approach. However, until now, immunotherapy displayed negative results on glioblastoma. Therefore, the use of auxiliary therapies plays a key role to produce specific and long-lasting antitumor immune response against glioblastoma-immune evasion. PTT can be an intriguing auxiliary cytotoxic approach due to the release of tumor-associated antigens and production of reactive oxygen species, which can strongly stimulate immune cells specifically against glioblastoma. We investigated the migration of human immune cells towards glioblastoma spheroids exposed to GQDs-mediated PTT. We found a rapid migration, which was associated with an increased production of reactive oxygen species from spheroids. Our evidence indicates that PTT can induce a strong and durable immune response specifically against glioblastoma, enhancing the efficacy of immunotherapy.

Methods

Characterization of GQDs

Graphene quantum dots in powder were purchased from ACS Material. GQDs were dissolved in double-distilled water (MilliQ) at a final concentration of 1 mg/mL. After

dissolution, GQDs were microscopically and spectroscopically characterized. Transmission electron microscopy (TEM) was performed with a Zeiss Libra 120 electron microscope. For TEM, 50 μg/mL of GQDs was spotted on a TEM tab and let dry at room temperature. Dynamic light scattering measurements were performed with Zetasizer Nano ZS (Malvern), equipped with a 633 nm He–Ne laser and operating at an angle of 173°. UV-transparent cuvettes (Malvern) have been used for experiments with a sample volume of 500 μL and a concentration of 100 μg/mL. The measurements were performed at a fixed position (4.65 mm) with an automatic attenuator. For each sample, three measurements were averaged, and the diffusion coefficient *D* has been retrieved through cumulants analysis from autocorrelation functions. The equivalent hydrodynamic radius (Z-Average size) was obtained by the Stokes–Einstein equation. Data analysis was performed by Malvern Zetasizer software. Optical density (OD) and fluorescence intensity were obtained using a Cytation 3 Cell Imaging Multi-Mode Reader (Biotek). OD was recorded from 230 to 800 nm. Fluorescence intensity spectra were obtained by using excitation wavelengths from 260 to 480 nm with a step of 20 nm and reading the emission from 300 to 700 nm with a step of 5 nm. Fluorescence intensity spectra were normalized to their corresponding maximum emission. To perform atomic force microscopy (AFM) imaging, GQDs were diluted at a final concentration of 10 μg/mL. They were then deposited on mica slides and dried for AFM with a NanoWizard II (JPK Instruments). The images were acquired using silicon cantilevers with high aspect-ratio conical silicon tips (CSC36 Mikro-Masch) having an end radius of about 10 nm, a half conical angle of 20°, and a spring constant of 0.6 N/m. Scan areas of 3×3 μm were imaged. The chemical analysis of the GQDs was carried out using Attenuated Total Reflectance-Fourier Transform Infrared spectroscopy (ATR-FTIR) by Spectrum One spectrometer (Perkin Elmer). The material under investigation was directly laid upon the ATR crystal and the spectra were recorded in the wave number range of 4000–550 cm^{-1}.

Near-infrared laser characterization

A near-infrared laser (LaserEver) focused at 808 nm was used to perform photothermal treatments on cells. First, the laser was characterized by evaluating the laser power at every current intensity by using a power meter. The spot of the laser had a diameter of 0.8 cm. The power density was evaluated by normalizing the laser power to the area of the spot. To test the photothermal effect of GQDs, different concentrations of the nanomaterials were used ranging from 50 to 250 μg/mL. GQDs were irradiated at a power density of 6 W/cm^2 for 5 min. Thermal increase was monitored using a thermal camera (Optris) focused on the well containing irradiated nanoparticles.

Cell culture

U87 human glioblastoma cells and human fibroblasts were purchased from the American Type Culture Collection (ATCC). Cells were maintained in Dulbecco's modified Eagle's medium (Sigma-Aldrich) supplemented with 10% fetal bovine serum (FBS, EuroClone), 2% penicillin–streptomycin (Sigma-Aldrich), and 2% L-glutamine (Sigma-Aldrich). Cells were kept in T75 flasks (Corning) at at 37 °C, 5% CO_2 for further treatments.

Cell viability measurements on 2D model

To measure cell viability on 2D cultures, cells were seeded on 96-well plates (Corning) at a seeding density of 1×10^5 cells/well. Plates were then incubated at 37 °C, 5% CO_2. To test the biocompatibility of GQDs, nanoparticles were administered at concentrations ranging from 50 to 250 μg/mL. After 24 h of incubation, viability was measured using CellTiter-Glo® (Promega). Briefly, an amount of CellTiter-Glo® reagent equal to the volume of culture medium was added to each well. Then, the plate was orbitally shaken for 2 min to ensure complete cell lysis and incubated in the dark at room temperature for 10 min. After incubation, luminescence was recorded using Cytation 3. Results were reported as % of control (untreated) cells. To evaluate the concentration inhibiting 50% of cell growth (IC50), doxorubicin (DOX) or temozolomide (TMZ) was administered to glioblastoma cells at different concentrations. For DOX, concentration ranged from 0.5 to 10 μM. For TMZ, concentration ranged from 62.5 to 1000 μg/mL. Untreated cells were used as a control group. Cells were then incubated at 37 °C—5% CO_2 for 48 h, then the viability was measured using CellTiter-Glo® as described above. Results were reported as % of control (untreated) cells. The IC50 was determined by fitting with Logger Pro software the experimental results. To evaluate the combined effect of chemotherapeutic drugs and graphene quantum dots (GQDs), cells were incubated with GQDs at different concentrations ranging from 50 to 250 μg/mL. After 24 h of incubation, GQDs were removed, and chemotherapeutic agents were added at half of their IC50. After further incubation, viability was measured using CellTiter-Glo® as described above.

Confocal microscopy on 2D model

Confocal microscopy images of 2D cell cultures were acquired with an inverted microscope (Nikon A1 MP+, Nikon). Cells were seeded on sterile chamber slides (Ibidi) at a concentration of 1×10^6 cell/mL and then incubated at 37 °C, 5% CO_2. After 24 h of incubation, GQDs were administered to cells at the highest tested concentration. For both 6-dodecanoyl-2-dimethylamino-naphthalene (Laurdan) measurements and DOX uptake, GQDs were removed, and the cells were resuspended in a fresh medium containing Laurdan or DOX at a final concentration of 1 μM. Confocal images were acquired at 37 °C for all measurements. For Laurdan excitation, cells were imaged with a wavelength of 400 nm. Laurdan is a fluorescent probe capable of detecting and distinguishing gel phase and liquid phase of the cell membrane. Laurdan intensity images were recorded simultaneously with emissions in the ranges of 425–475 nm (gel phase) and 500–550 nm (liquid phase). To quantify the images collected in this way, Fiji (ImageJ) software was used. The intensities of the two different channels were calculated, and the generalized polarization (GP) index was calculated as previously reported. For DOX uptake measurements, images were acquired after 1 h of incubation with DOX. The excitation and emission wavelengths were, respectively, 488 nm and 590 nm. To quantify the uptake, Fiji (ImageJ) software was used by measuring the fluorescence intensity of DOX. Data were normalized by cells treated with chemotherapeutic agent alone.

Spheroid preparation, growth and viability

For spheroid preparation, cells were seeded on 96-well, round bottom, ultra-low attachment plates (Corning) at a density of 0.25×10^5 cells/mL. The plate was centrifuged

at 300×*g* for 3 min to ensure the confluence of cells to the center of the wells. The so-formed single spheroids were incubated for three days at 37 °C with 5% CO_2. Spheroids were treated for 2 weeks with GQDs at 200 μg/mL with or without chemotherapy administration. Culture medium was changed with fresh medium containing the same concentration of nanoparticles and chemotherapeuticals every 3 days. For photothermal treatments, spheroids were irradiated with an 808 nm laser for 5 min at 6 W/cm^2. Transmittance images of spheroids were collected using Cytation 3, and spheroid growth in terms of area was analyzed with INSIDIA 2.0 as described elsewhere. Spheroid viability was evaluated at 7 and 14 days from the beginning of the experiments using CellTiter-Glo® luminescent assay as described above. For spheroid growth, data were normalized by the area at day 0 for each treatment. For viability, results were reported as % of control (untreated) spheroids.

Changes in membrane permeability on spheroids

To test changes in membrane permeability on the 3D model, the uptake of calcein-AM (ThermoFisher) was measured. Briefly, spheroids were incubated with GQDs at a concentration of 200 μg/mL. After 24 h of incubation, spheroids were irradiated with an 808 nm laser at 6 W/cm^2 for 5 min. Then, calcein was added at a final concentration of 10 μM and incubated in a Cytation 3 for 30 min at 37 °C. Fluorescence intensity was recorded by exciting at 488 nm and recording emission at 525 nm. Data were then normalized by the fluorescence intensity at the beginning. To evaluate fluorescence intensity of calcein, spheroids at different timepoints were collected for each condition (untreated, incubated with GQDs and incubated with GQDs and irradiated) and imaged with confocal microscopy using Nikon A1 MP+.

Production of reactive oxygen species on glioblastoma spheroids

For the detection of reactive oxygen species (ROS), the fluorinated derivative of 2′,7′-dichlorofluorescein (H_2DCFDA, Sigma-Aldrich) was employed. This probe is non-fluorescent until the acetate groups are removed by intracellular esterases and oxidation occurs within cells. Thus, oxidation can be detected by monitoring the increase in fluorescence intensity. Spheroids were treated with GQDs at 200 μg/mL for 24 h. After the treatment, cells were irradiated with an 808 nm laser with a power density of 6 W/cm^2 for 5 min. After a recovery time of 30 min, the medium containing GQDs was carefully washed and replaced with PBS containing 10 μM H_2DCFDA. Cells were incubated for an additional hour at 37 °C, 5% CO_2. PBS containing H_2DCFDA was then removed, and spheroids were resuspended in complete medium. Fluorescence intensity of H_2DCFDA was recorded by using a Cytation 3 by exciting at 495 nm and recording emission at 528 nm. Results were expressed as % of control (untreated) spheroids.

Uptake of chemotherapeutic drug on spheroids

The uptake of DOX through tumor spheroids was evaluated via quantification of fluorescence intensity in confocal microscopy images of spheroids. Briefly, 3D models were incubated with GQDs for 24 h. After incubation, DOX was added and photothermal irradiation was performed with an 808 nm laser. Spheroids were then incubated with calcein for 20 min, and then images were acquired with Nikon A1 MP+ by exciting at

488 nm and reading at 525 nm (calcein) and by reading emission at 590 nm (DOX). Uptake of DOX was evaluated in terms of fluorescence intensity and penetration depth. Uptake was compared to cells incubated with only DOX or with DOX and GQDs.

Migration of THP-1 towards glioblastoma spheroids

To evaluate migration of THP-1 human monocytic cell line towards cancer region, U87 spheroids were treated with GQDs at 200 μg/mL. After 24 h of incubation, spheroids were irradiated with an 808 nm laser for 5 min at 6 W/cm^2. After a recovery time of 30 min, spheroids were co-cultured with THP-1 cells stained with Red Long-Term Cell Tracer Kit (Enzo), by following manufacturer's instructions. Briefly, cells were centrifuged for 5 min at 400×*g*, and then supernatant was discarded. Cells were then resuspended in 1 mL of Labeling Buffer. An equal volume of 2XCyto-ID™ RED Tracer Dye was added to the cell suspension. The suspension was incubated for 5 min. Then, Stop Buffer was added to block the reaction. Finally, cells were centrifuged and resuspended in a culture medium. Images were acquired in bright field (spheroids) and Texas red channel with a Cytation 3 for 48 h at 37 °C, 5% CO_2.

Statistical analysis

Statistical analysis was performed using one-way ANOVA, followed by Tukey's post-hoc test. Differences were considered significant when $p < 0.01$.

Abbreviations

2D	Two dimensional
3D	Three dimensional
ANOVA	Analysis of variance
ATR-FTIR	Attenuated Total Reflectance-Fourier Transform Infrared spectroscopy
DLS	Dynamic light scattering
DOX	Doxorubicin
FDA	Food and Drug Administration
GQDs	Graphene quantum dots
IC50	Inhibiting 50% of cell growth
NIR	Near-infrared light
OD	Optical density
PBS	Phosphate-buffered saline
PDT	Photodynamic therapy
PTT	Photothermal therapy
ROS	Reactive oxygen species
RT	Room temperature
TEM	Transmission Electron Microscopy
TMZ	Temozolomide
GP	Generalized polarization
UV	Ultraviolet

Acknowledgements

We would like to acknowledge the contribution of 3D Bioprinting Research Core Facility G-STeP of the Fondazione Policlinico Universitario "A. Gemelli" IRCCS for sample processing.

Author contributions

GP and GF performed the experiments. AA and GP realized the 3D bioprinting cellular models. GP, VP, MDS, and MP analyzed and interpreted the data. MP designed the experiments. All authors read and approved the final manuscript.

Funding

The research leading to these results has received funding from AIRC under IG 2019—ID. 23124 project—P.I. Massimiliano Papi and from AIRC Grant to Giordano Perini 26918-2021.

Availability of data and materials

The datasets used and/or analyzed during the current study are available from the corresponding author on reasonable request.

Declarations

Ethics approval and consent to participate
Not applicable.

Consent for publication
Not applicable.

Competing interests
The authors declare that they have no competing interests.

Received: 25 November 2022 Accepted: 15 February 2023
Published online: 24 February 2023

References

Abadi B, Yazdanpanah N, Nokhodchi A, Rezaei N (2021) Smart biomaterials to enhance the efficiency of immunotherapy in glioblastoma: state of the art and future perspectives. Adv Drug Deliv Rev 179:114035
Ampie L, Woolf EC, Dardis C (2015) Immunotherapeutic advancements for glioblastoma. Front Oncol 5:12
Anthony C, Mladkova-Suchy N, Adamson DC (2019) The evolving role of antiangiogenic therapies in glioblastoma multiforme: current clinical significance and future potential. Expert Opin Investig Drugs 28:787–797
Bacon M, Bradley SJ, Nann T (2014) Graphene quantum dots. Part Part Syst Charact 31:415–428
Bausart M, Préat V, Malfanti A (2022) Immunotherapy for glioblastoma: the promise of combination strategies. J Exp Clin Cancer Res 41:1–22
Bianchetti G et al (2019) Red blood cells membrane micropolarity as a novel diagnostic indicator of type 1 and type 2 diabetes. Anal Chim Acta X 3:100030
Bugno J, Hsu H-J, Pearson RM, Noh H, Hong S (2016) Size and surface charge of engineered poly (amidoamine) dendrimers modulate tumor accumulation and penetration: a model study using multicellular tumor spheroids. Mol Pharm 13:2155–2163
Chang M, Hou Z, Wang M, Li C, Lin J (2021) Recent advances in hyperthermia therapy-based synergistic immunotherapy. Adv Mater 33:2004788
Chongsathidkiet P et al (2018) Sequestration of T cells in bone marrow in the setting of glioblastoma and other intracranial tumors. Nat Med 24:1459–1468
Costa EC et al (2016) 3D tumor spheroids: an overview on the tools and techniques used for their analysis. Biotechnol Adv 34:1427–1441
Ding M et al (2021) A NO/ROS/RNS cascaded-releasing nano-platform for gas/PDT/PTT/immunotherapy of tumors. Biomater Sci 9:5824–5840
Fecci PE, Sampson JH (2019) The current state of immunotherapy for gliomas: an eye toward the future: JNSPG 75th anniversary invited review article. J Neurosurg 131:657–666
Forlani G et al (2021) CIITA-transduced glioblastoma cells uncover a rich repertoire of clinically relevant tumor-associated HLA-II antigens. Mol Cell Proteom 20:100032
Hanada S et al (2014) Cell-based in vitro blood–brain barrier model can rapidly evaluate nanoparticles' brain permeability in association with particle size and surface modification. Int J Mol Sci 15:1812–1825
Heimberger AB, Sampson JH (2010) Immunotherapy coming of age: what will it take to make it standard of care for glioblastoma? Neuro Oncol 13:3–13
Huai J et al (2013) TNFα-induced lysosomal membrane permeability is downstream of MOMP and triggered by caspase-mediated NDUFS1 cleavage and ROS formation. J Cell Sci 126:4015–4025
Huang Z et al (2014) Quantum confinement in graphene quantum dots. Phys Status Solidi Rapid Res Lett 8:436–440
Jauković A et al (2020) Specificity of 3D MSC spheroids microenvironment: impact on MSC behavior and properties. Stem Cell Rev Rep 16:853–875
Jiapaer S, Furuta T, Tanaka S, Kitabayashi T, Nakada M (2018) Potential strategies overcoming the temozolomide resistance for glioblastoma. Neurol Med Chir (Tokyo) 58:405
Kim HS, Lee DY (2018) Near-infrared-responsive cancer photothermal and photodynamic therapy using gold nanoparticles. Polymers (Basel) 10:961
Kowaltowski AJ, Castilho RF, Vercesi AE (2001) Mitochondrial permeability transition and oxidative stress. FEBS Lett 495:12–15
Lazzari G et al (2019) Light sheet fluorescence microscopy versus confocal microscopy: in quest of a suitable tool to assess drug and nanomedicine penetration into multicellular tumor spheroids. Eur J Pharm Biopharm 142:195–203
Lee SY (2016) Temozolomide resistance in glioblastoma multiforme. Genes Dis 3:198–210
Lemasters JJ (2007) Modulation of mitochondrial membrane permeability in pathogenesis, autophagy and control of metabolism. J Gastroenterol Hepatol 22:S31–S37
Lim M, Xia Y, Bettegowda C, Weller M (2018) Current state of immunotherapy for glioblastoma. Nat Rev Clin Oncol 15:422–442
Liu S, Pan X, Liu H (2020a) Two-dimensional nanomaterials for photothermal therapy. Angew Chemie 132:5943–5953
Liu H et al (2020b) Magnetic-induced graphene quantum dots for imaging-guided photothermal therapy in the second near-infrared window. Biomaterials 232:119700
Longati P et al (2013) 3D pancreatic carcinoma spheroids induce a matrix-rich, chemoresistant phenotype offering a better model for drug testing. BMC Cancer 13:95
Ma HL et al (2012) Multicellular tumor spheroids as an in vivo-like tumor model for three-dimensional imaging of chemotherapeutic and nano material cellular penetration. Mol Imaging 11:487–498
Mansur HS (2010) Quantum dots and nanocomposites. WIREs Nanomed Nanobiotechnol 2:113–129

Markovic ZM et al (2012) Graphene quantum dots as autophagy-inducing photodynamic agents. Biomaterials 33:7084–7092
Moriconi C et al (2017) INSIDIA: a FIJI macro delivering high-throughput and high-content spheroid invasion analysis. Biotechnol J 12:1700140
Nurunnabi M, Khatun Z, Reeck GR, Lee DY, Lee YK (2014) Photoluminescent graphene nanoparticles for cancer phototherapy and imaging. ACS Appl Mater Interfaces 6:12413–12421
Palmieri V et al (2019) Biocompatible: *N*-acetyl cysteine reduces graphene oxide and persists at the surface as a green radical scavenger. Chem Commun 55:4186–4189
Palmieri V et al (2021) In situ *N*-acetylcysteine release from polyvinyl alcohol film for moisture-activated food packaging. Food Packag Shelf Life 29:100694
Parasassi T, De Stasio G, d'Ubaldo A, Gratton E (1990) Phase fluctuation in phospholipid membranes revealed by Laurdan fluorescence. Biophys J 57:1179–1186
Parasassi T, Krasnowska EK, Bagatolli L, Gratton E (1998) Laurdan and Prodan as polarity-sensitive fluorescent membrane probes. J Fluoresc 8:365–373
Perini G et al (2020a) Enhanced chemotherapy for glioblastoma multiforme mediated by functionalized graphene quantum dots. Mater (Basel, Switzerland) 13:4139
Perini G et al (2020b) Unravelling the potential of graphene quantum dots in biomedicine and neuroscience. Int J Mol Sci. https://doi.org/10.3390/ijms21103712
Perini G et al (2020c) Graphene quantum dots' surface chemistry modulates the sensitivity of glioblastoma cells to chemotherapeutics. Int J Mol Sci 21:6301
Perini G et al (2021a) Inhibiting the growth of 3D brain cancer models with bio-coronated liposomal temozolomide. Pharmaceutics 13:378
Perini G et al (2021b) Functionalized graphene quantum dots modulate malignancy of glioblastoma multiforme by downregulating neurospheres formation. C 7:4
Perini G et al (2022a) INSIDIA 2.0 high-throughput analysis of 3D cancer models: multiparametric quantification of graphene quantum dots photothermal therapy for glioblastoma and pancreatic cancer. Int J Mol Sci 23:3217
Perini G et al (2022b) Advanced usage of Ti3C2Tx MXenes for photothermal therapy on different 3D breast cancer models. Biomed Pharmacother 153:113496
Pickl M, Ries CH (2009) Comparison of 3D and 2D tumor models reveals enhanced HER2 activation in 3D associated with an increased response to trastuzumab. Oncogene 28:461–468
Pierangeli D et al (2020) Living optical random neural network with three dimensional tumor spheroids for cancer morphodynamics. Commun Phys 3:160
Priwitaningrum DL et al (2016) Tumor stroma-containing 3D spheroid arrays: a tool to study nanoparticle penetration. J Control Release 244:257–268
Qian H, Shao Y (2022) Research progress of photothermal-mediated immunotherapy in the prevention of tumor recurrence and metastases. J Nanopart Res 24:1–12
Rong L et al (2019) Iron chelated melanin-like nanoparticles for tumor-associated macrophage repolarization and cancer therapy. Biomaterials 225:119515
Rosenkranz A et al (2021) Laser-mediated antibacterial effects of few- and multi-layer Ti3C2Tx MXenes. Appl Surf Sci 567:150795
Rubenstein JL et al (2000) Anti-VEGF antibody treatment of glioblastoma prolongs survival but results in increased vascular cooption. Neoplasia 2:306–314
Sánchez-Romero N, Schophuizen CMS, Giménez I, Masereeuw R (2016) In vitro systems to study nephropharmacology: 2D versus 3D models. Eur J Pharmacol 790:36–45
Sang D et al (2020) Disrupted intracellular redox balance with enhanced ROS generation and sensitive drug release for cancer therapy. Biomater Sci 8:6045–6055
Stupp R et al (2005) Radiotherapy plus concomitant and adjuvant temozolomide for glioblastoma. N Engl J Med 352:987–996
Sui X et al (2016) Graphene quantum dots enhance anticancer activity of cisplatin via increasing its cellular and nuclear uptake. Nanomed Nanotechnol Biol Med 12:1997–2006
Sung SY et al (2017) Photodynamic graphene quantum dot: reduction condition regulated photoactivity and size dependent efficacy. ACS Appl Mater Interfaces 8:25865–25874
Urbańska K, Sokołowska J, Szmidt M, Sysa P (2014) Glioblastoma multiforme—an overview. Contemp Oncol (Poznan, Poland) 18:307–312
Utkin YN (2018) Brain and quantum dots: benefits of nanotechnology for healthy and diseased brain. Cent Nerv Syst Agents Med Chem 18:193–205
Wang H et al (2019) Nitrogen and boron dual-doped graphene quantum dots for near-infrared second window imaging and photothermal therapy. Appl Mater Today 14:108–117
Wang C, Cheng X, Peng H, Zhang Y (2022) NIR-triggered and ROS-boosted nanoplatform for enhanced chemo/PDT/PTT synergistic therapy of sorafenib in hepatocellular carcinoma. Nanoscale Res Lett 17:1–16
Woroniecka K, Fecci PE (2018) T-cell exhaustion in glioblastoma. Oncotarget 9:35287
Yang G-G et al (2019) Multifunctional low-temperature photothermal nanodrug with in vivo clearance, ROS-scavenging and anti-inflammatory abilities. Biomaterials 216:119280
Yao H et al (2020) Underlying mechanisms of reactive oxygen species and oxidative stress photoinduced by graphene and its surface-functionalized derivatives. Environ Sci Nano 7:782–792
Zhi D, Yang T, O'hagan J, Zhang S, Donnelly RF (2020) Photothermal therapy. J Control Release 325:52–71

Publisher's Note